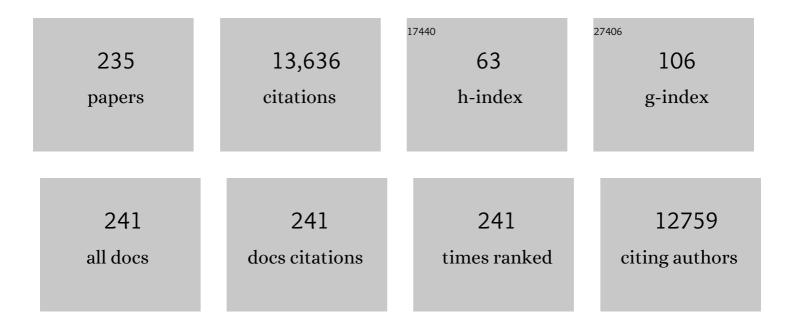
List of Publications by Year in descending order

Source: https://exaly.com/author-pdf/2016712/publications.pdf Version: 2024-02-01



OIN-FEN CU

#	Article	IF	CITATIONS
1	A two-dimensional zeolitic imidazolate framework with a cushion-shaped cavity for CO2 adsorption. Chemical Communications, 2013, 49, 9500.	4.1	514
2	Transition Metal Borides: Superhard versus Ultraâ€incompressible. Advanced Materials, 2008, 20, 3620-3626.	21.0	467
3	Discriminative Separation of Gases by a "Molecular Trapdoor―Mechanism in Chabazite Zeolites. Journal of the American Chemical Society, 2012, 134, 19246-19253.	13.7	321
4	Atomic cobalt as an efficient electrocatalyst in sulfur cathodes for superior room-temperature sodium-sulfur batteries. Nature Communications, 2018, 9, 4082.	12.8	305
5	Hydrogen Storage Materials for Mobile and Stationary Applications: Current State of the Art. ChemSusChem, 2015, 8, 2789-2825.	6.8	302
6	Reversible structural evolution of sodium-rich rhombohedral Prussian blue for sodium-ion batteries. Nature Communications, 2020, 11, 980.	12.8	283
7	Achieving High-Performance Room-Temperature Sodium–Sulfur Batteries With S@Interconnected Mesoporous Carbon Hollow Nanospheres. Journal of the American Chemical Society, 2016, 138, 16576-16579.	13.7	280
8	NASICON-type air-stable and all-climate cathode for sodium-ion batteries with low cost and high-power density. Nature Communications, 2019, 10, 1480.	12.8	260
9	Atomic Engineering Catalyzed MnO ₂ Electrolysis Kinetics for a Hybrid Aqueous Battery with High Power and Energy Density. Advanced Materials, 2020, 32, e2001894.	21.0	221
10	Comprehensive Determination of Kinetic Parameters in Solid-State Phase Transitions: An Extended Jonhson–Mehl–Avrami–Kolomogorov Model with Analytical Solutions. Crystal Growth and Design, 2016, 16, 2404-2415.	3.0	206
11	The effect of different binders on electrochemical properties of LiNi1/3Mn1/3Co1/3O2 cathode material in lithium ion batteries. Journal of Power Sources, 2013, 225, 172-178.	7.8	202
12	Insight into Si poisoning on grain refinement of Al-Si/Al-5Ti-B system. Acta Materialia, 2020, 187, 51-65.	7.9	195
13	<i>In Situ</i> Growth of Layered Bimetallic ZnCo Hydroxide Nanosheets for High-Performance All-Solid-State Pseudocapacitor. ACS Nano, 2018, 12, 2968-2979.	14.6	193
14	Three-Dimensional MOFs@MXene Aerogel Composite Derived MXene Threaded Hollow Carbon Confined CoS Nanoparticles toward Advanced Alkali-Ion Batteries. ACS Nano, 2021, 15, 3228-3240.	14.6	189
15	Sandwichâ€Like Ultrathin TiS ₂ Nanosheets Confined within N, S Codoped Porous Carbon as an Effective Polysulfide Promoter in Lithiumâ€Sulfur Batteries. Advanced Energy Materials, 2019, 9, 1901872.	19.5	186
16	Ultrathin water-stable metal-organic framework membranes for ion separation. Science Advances, 2020, 6, eaay3998.	10.3	179
17	Hydrothermal Synthesis of Metal–Polyphenol Coordination Crystals and Their Derived Metal/Nâ€doped Carbon Composites for Oxygen Electrocatalysis. Angewandte Chemie - International Edition, 2016, 55, 12470-12474.	13.8	178
18	Hydrogenation Synthesis of Blue TiO ₂ for High-Performance Lithium-Ion Batteries. Journal of Physical Chemistry C, 2014, 118, 8824-8830.	3.1	167

#	Article	IF	CITATIONS
19	Multifunctional conducing polymer coated Na1+MnFe(CN)6 cathode for sodium-ion batteries with superior performance via a facile and one-step chemistry approach. Nano Energy, 2015, 13, 200-207.	16.0	165
20	Facile Method To Synthesize Na-Enriched Na _{1+<i>x</i>} FeFe(CN) ₆ Frameworks as Cathode with Superior Electrochemical Performance for Sodium-Ion Batteries. Chemistry of Materials, 2015, 27, 1997-2003.	6.7	163
21	Molten Salt-Directed Catalytic Synthesis of 2D Layered Transition-Metal Nitrides for Efficient Hydrogen Evolution. CheM, 2020, 6, 2382-2394.	11.7	163
22	Carbon oated Na _{3.32} Fe _{2.34} (P ₂ O ₇) ₂ Cathode Material for Highâ€Rate and Longâ€Life Sodiumâ€Ion Batteries. Advanced Materials, 2017, 29, 1605535	.21.0	161
23	Ultrathin VSe ₂ Nanosheets with Fast Ion Diffusion and Robust Structural Stability for Rechargeable Zincâ€ion Battery Cathode. Small, 2020, 16, e2000698.	10.0	154
24	Electronâ€6tate Confinement of Polysulfides for Highly Stable Sodium–Sulfur Batteries. Advanced Materials, 2020, 32, e1907557.	21.0	150
25	Nickel sulfide nanocrystals on nitrogen-doped porous carbon nanotubes with high-efficiency electrocatalysis for room-temperature sodium-sulfur batteries. Nature Communications, 2019, 10, 4793.	12.8	147
26	Facile Synthesis of Hierarchical Hollow CoP@C Composites with Superior Performance for Sodium and Potassium Storage. Angewandte Chemie - International Edition, 2020, 59, 5159-5164.	13.8	142
27	Multi-shell hollow structured Sb2S3 for sodium-ion batteries with enhanced energy density. Nano Energy, 2019, 60, 591-599.	16.0	136
28	Charge Transfer in Ultrafine LDH Nanosheets/Graphene Interface with Superior Capacitive Energy Storage Performance. ACS Applied Materials & Interfaces, 2017, 9, 37645-37654.	8.0	134
29	Thermally treated zeolitic imidazolate framework-8 (ZIF-8) for visible light photocatalytic degradation of gaseous formaldehyde. Chemical Science, 2020, 11, 6670-6681.	7.4	130
30	Atomically Dispersed Iron Metal Site in a Porphyrin-Based Metal–Organic Framework for Photocatalytic Nitrogen Fixation. ACS Nano, 2021, 15, 9670-9678.	14.6	127
31	A Highâ€Kinetics Sulfur Cathode with a Highly Efficient Mechanism for Superior Roomâ€Temperature Na–S Batteries. Advanced Materials, 2020, 32, e1906700.	21.0	126
32	The influence of Ni and Zn additions on microstructure and phase transformations in Sn–0.7Cu/Cu solder joints. Acta Materialia, 2015, 83, 357-371.	7.9	119
33	Faster Activation and Slower Capacity/Voltage Fading: A Bifunctional Urea Treatment on Lithiumâ€Rich Cathode Materials. Advanced Functional Materials, 2020, 30, 1909192.	14.9	117
34	Incorporation of Homochirality into a Zeolitic Imidazolate Framework Membrane for Efficient Chiral Separation. Angewandte Chemie - International Edition, 2018, 57, 17130-17134.	13.8	113
35	MXene derived TiS2 nanosheets for high-rate and long-life sodium-ion capacitors. Energy Storage Materials, 2020, 26, 550-559.	18.0	108
36	Multiangular Rod-Shaped Na _{0.44} MnO ₂ as Cathode Materials with High Rate and Long Life for Sodium-Ion Batteries. ACS Applied Materials & Interfaces, 2017, 9, 3644-3652.	8.0	107

#	Article	IF	CITATIONS
37	Maximizing sinusoidal channels of HZSM-5 for high shape-selectivity to p-xylene. Nature Communications, 2019, 10, 4348.	12.8	102
38	P2-type Na _{2/3} Ni _{1/3} Mn _{2/3} O ₂ as a cathode material with high-rate and long-life for sodium ion storage. Journal of Materials Chemistry A, 2019, 7, 9215-9221.	10.3	102
39	A Novel Graphene Oxide Wrapped Na ₂ Fe ₂ (SO ₄) ₃ /C Cathode Composite for Long Life and High Energy Density Sodium″on Batteries. Advanced Energy Materials, 2018, 8, 1800944.	19.5	101
40	Development and Investigation of a NASICONâ€Type Highâ€Voltage Cathode Material for Highâ€Power Sodiumâ€Ion Batteries. Angewandte Chemie - International Edition, 2020, 59, 2449-2456.	13.8	101
41	Electrocatalyzing S Cathodes <i>via</i> Multisulfiphilic Sites for Superior Room-Temperature Sodium–Sulfur Batteries. ACS Nano, 2020, 14, 7259-7268.	14.6	100
42	The cycling stability of the in situ formed Mg-based nanocomposite catalyzed by YH ₂ . Journal of Materials Chemistry A, 2017, 5, 17532-17543.	10.3	93
43	Origin of large electric-field-induced strain in pseudo-cubic BiFeO3–BaTiO3 ceramics. Acta Materialia, 2020, 197, 1-9.	7.9	93
44	A Hydrostable Cathode Material Based on the Layered P2@P3 Composite that Shows Redox Behavior for Copper in Highâ€Rate and Longâ€Cycling Sodiumâ€Ion Batteries. Angewandte Chemie - International Edition, 2019, 58, 1412-1416.	13.8	92
45	Facile synthesis of CuBTC and its graphene oxide composites as efficient adsorbents for CO2 capture. Chemical Engineering Journal, 2020, 393, 124666.	12.7	85
46	A 12R long-period stacking-ordered structure in a Mg-Ni-Y alloy. Journal of Materials Science and Technology, 2018, 34, 2235-2239.	10.7	83
47	Structure and decomposition of zinc borohydride ammonia adduct: towards a pure hydrogen release. Energy and Environmental Science, 2012, 5, 7590.	30.8	82
48	In-situ observation of grain refinement dynamics of hypoeutectic Al-Si alloy inoculated by Al-Ti-Nb-B alloy. Scripta Materialia, 2020, 187, 142-147.	5.2	82
49	Self-Assembled Hydrophobic/Hydrophilic Porphyrin-Ti ₃ C ₂ T <i>_x</i> MXene Janus Membrane for Dual-Functional Enabled Photothermal Desalination. ACS Applied Materials & Interfaces, 2021, 13, 3762-3770.	8.0	82
50	The mechanism for the enhanced piezoelectricity in multi-elements doped (K,Na)NbO3 ceramics. Nature Communications, 2021, 12, 881.	12.8	82
51	Revealing the Origin of Improved Reversible Capacity of Dual-Shell Bismuth Boxes Anode for Potassium-Ion Batteries. Matter, 2019, 1, 1681-1693.	10.0	81
52	General Synthesis of Singleâ€Atom Catalysts for Hydrogen Evolution Reactions and Roomâ€Temperature Naâ€S Batteries. Angewandte Chemie - International Edition, 2020, 59, 22171-22178.	13.8	80
53	A Mo5N6 electrocatalyst for efficient Na2S electrodeposition in room-temperature sodium-sulfur batteries. Nature Communications, 2021, 12, 7195.	12.8	80
54	A Cation and Anion Dual Doping Strategy for the Elevation of Titanium Redox Potential for Highâ€Power Sodiumâ€ion Batteries. Angewandte Chemie - International Edition, 2020, 59, 12076-12083.	13.8	78

#	Article	IF	CITATIONS
55	Enhancing the High Rate Capability and Cycling Stability of LiMn ₂ O ₄ by Coating of Solid-State Electrolyte LiNbO ₃ . ACS Applied Materials & Interfaces, 2014, 6, 22155-22165.	8.0	75
56	Impact of pressure on physicochemical properties of starch dispersions. Food Hydrocolloids, 2017, 68, 164-177.	10.7	74
57	Directly anchoring Fe3C nanoclusters and FeNx sites in ordered mesoporous nitrogen-doped graphitic carbons to boost electrocatalytic oxygen reduction. Carbon, 2017, 121, 143-153.	10.3	71
58	In-situ synchrotron X-ray diffraction investigation on hydrogen-induced decomposition of long period stacking ordered structure in Mg–Ni–Y system. Scripta Materialia, 2017, 127, 102-107.	5.2	70
59	Transition metal cation-exchanged SSZ-13 zeolites for CO2 capture and separation from N2. Chemical Engineering Journal, 2019, 370, 1450-1458.	12.7	70
60	Efficient Gating of Ion Transport in Threeâ€Dimensional Metal–Organic Framework Subâ€Nanochannels with Confined Lightâ€Responsive Azobenzene Molecules. Angewandte Chemie - International Edition, 2020, 59, 13051-13056.	13.8	70
61	Photocatalytic Bacterial Inactivation by a Rape Pollen-MoS ₂ Biohybrid Catalyst: Synergetic Effects and Inactivation Mechanisms. Environmental Science & Technology, 2020, 54, 537-549.	10.0	69
62	Achievement in grain-refining hypoeutectic Al-Si alloys with Nb. Scripta Materialia, 2019, 160, 75-80.	5.2	68
63	Ice-Assisted Synthesis of Highly Crystallized Prussian Blue Analogues for All-Climate and Long-Calendar-Life Sodium Ion Batteries. Nano Letters, 2022, 22, 1302-1310.	9.1	68
64	Thermodynamic investigation on phase formation in the Al–Si rich region of Al–Si–Ti system. Materials and Design, 2016, 102, 78-90.	7.0	67
65	Solving Key Challenges in Battery Research Using In Situ Synchrotron and Neutron Techniques. Advanced Energy Materials, 2017, 7, 1602831.	19.5	67
66	Achieving superior cycling stability by <i>in situ</i> forming NdH ₂ –Mg–Mg ₂ Ni nanocomposites. Journal of Materials Chemistry A, 2018, 6, 23308-23317.	10.3	67
67	Stress Distortion Restraint to Boost the Sodium Ion Storage Performance of a Novel Binary Hexacyanoferrate. Advanced Energy Materials, 2020, 10, 1903006.	19.5	67
68	Effect of Eliminating Water in Prussian Blue Cathode for Sodiumâ€lon Batteries. Advanced Functional Materials, 2022, 32, .	14.9	66
69	Phase transition and hydrogen storage properties of Mg17Ba2 compound. Journal of Alloys and Compounds, 2017, 690, 519-522.	5.5	65
70	A New Ammine Dual ation (Li, Mg) Borohydride: Synthesis, Structure, and Dehydrogenation Enhancement. Chemistry - A European Journal, 2012, 18, 6825-6834.	3.3	62
71	Insights into the composition exploration of novel hydrogen storage alloys: evaluation of the Mg–Ni–Nd–H phase diagram. Journal of Materials Chemistry A, 2017, 5, 3848-3864.	10.3	62
72	General Synthesis of Singleâ€Atom Catalysts for Hydrogen Evolution Reactions and Roomâ€Temperature Naâ€S Batteries. Angewandte Chemie, 2020, 132, 22355-22362.	2.0	62

#	Article	IF	CITATIONS
73	Understanding rhombohedral iron hexacyanoferrate with three different sodium positions for high power and long stability sodium-ion battery. Energy Storage Materials, 2020, 30, 42-51.	18.0	62
74	Complex Ammine Titanium(III) Borohydrides as Advanced Solid Hydrogen-Storage Materials with Favorable Dehydrogenation Properties. Chemistry of Materials, 2012, 24, 3370-3379.	6.7	61
75	Temperature-regulated guest admission and release in microporous materials. Nature Communications, 2017, 8, 15777.	12.8	60
76	A Layered Zn _{0.4} VOPO ₄ ·0.8H ₂ O Cathode for Robust and Stable Zn Ion Storage. ACS Applied Energy Materials, 2020, 3, 3919-3927.	5.1	60
77	Novel Subâ€5 nm Layered Niobium Phosphate Nanosheets for Highâ€Voltage, Cationâ€Intercalation Typed Electrochemical Energy Storage in Wearable Pseudocapacitors. Advanced Energy Materials, 2019, 9, 1900111.	19.5	57
78	In situ study starch gelatinization under ultra-high hydrostatic pressure using synchrotron SAXS. Food Hydrocolloids, 2016, 56, 58-61.	10.7	56
79	Phosphorusâ€Modulationâ€Triggered Surface Disorder in Titanium Dioxide Nanocrystals Enables Exceptional Sodiumâ€&torage Performance. Angewandte Chemie - International Edition, 2019, 58, 4022-4026.	13.8	56
80	Structure and hydrogenstorage properties of the first rare-earth metal borohydride ammoniate: Y(BH ₄) ₃ A·4NH ₃ . Journal of Materials Chemistry, 2012, 22, 1061-1068.	6.7	55
81	In-situ investigation of the hydrogen release mechanism in bulk Mg2NiH4. Journal of Power Sources, 2017, 341, 130-138.	7.8	55
82	Exfoliated Ni-Al LDH 2D nanosheets for intermediate temperature CO2 capture. Journal of Hazardous Materials, 2019, 374, 365-371.	12.4	55
83	Phase Equilibria, Crystal Structure and Hydriding/Dehydriding Mechanism of Nd4Mg80Ni8 Compound. Scientific Reports, 2015, 5, 15385.	3.3	53
84	Rapid Amorphization in Metastable CoSeO ₃ ·H ₂ O Nanosheets for Ultrafast Lithiation Kinetics. ACS Nano, 2018, 12, 5011-5020.	14.6	53
85	Catalytic Oxidation of K ₂ S via Atomic Co and Pyridinic N Synergy in Potassium–Sulfur Batteries. Journal of the American Chemical Society, 2021, 143, 16902-16907.	13.7	53
86	Ammine bimetallic (Na, Zn) borohydride for advanced chemical hydrogen storage. Journal of Materials Chemistry, 2012, 22, 7300.	6.7	52
87	Bottom-up Approach Design, Band Structure, and Lithium Storage Properties of Atomically Thin Î ³ -FeOOH Nanosheets. ACS Applied Materials & Interfaces, 2016, 8, 21334-21342.	8.0	49
88	Transitionâ€Metalâ€Containing Porphyrin Metal–Organic Frameworks as Ï€â€Backbonding Adsorbents for NO ₂ Removal. Angewandte Chemie - International Edition, 2020, 59, 19680-19683.	13.8	49
89	Continuous Carbon Channels Enable Full Naâ€Ion Accessibility for Superior Roomâ€Temperature Na–S Batteries. Advanced Materials, 2022, 34, e2108363.	21.0	49
90	Three-dimensional-network Li3V2(PO4)3/C composite as high rate lithium ion battery cathode material and its compatibility with ionic liquid electrolytes. Journal of Power Sources, 2014, 246, 124-131.	7.8	48

#	Article	IF	CITATIONS
91	Kinetics of the polymorphic phase transformation of Cu6Sn5. Acta Materialia, 2014, 69, 135-148.	7.9	48
92	Enhanced Potassium Ion Battery by Inducing Interlayer Anionic Ligands in MoS _{1.5} Se _{0.5} Nanosheets with Exploration of the Mechanism. Advanced Energy Materials, 2020, 10, 1904162.	19.5	48
93	In situ study of maize starch gelatinization under ultra-high hydrostatic pressure using X-ray diffraction. Carbohydrate Polymers, 2013, 97, 235-238.	10.2	47
94	Light metals decorated covalent triazine-based frameworks as a high capacity hydrogen storage medium. Journal of Materials Chemistry A, 2013, 1, 11705.	10.3	47
95	2D Titania–Carbon Superlattices Vertically Encapsulated in 3D Hollow Carbon Nanospheres Embedded with 0D TiO ₂ Quantum Dots for Exceptional Sodiumâ€Ion Storage. Angewandte Chemie - International Edition, 2019, 58, 14125-14128.	13.8	47
96	A Novel Approach to Highâ€Performance Aliovalentâ€6ubstituted Catalysts—2D Bimetallic MOFâ€Derived CeCuO <i>_x</i> Microsheets. Small, 2019, 15, e1903525.	10.0	46
97	Architecting Freestanding Sulfur Cathodes for Superior Roomâ€Temperature Na–S Batteries. Advanced Functional Materials, 2021, 31, 2102280.	14.9	46
98	A simple electrochemical cell for in-situ fundamental structural analysis using synchrotron X-ray powder diffraction. Journal of Power Sources, 2013, 244, 109-114.	7.8	45
99	Converting 3D rigid metal–organic frameworks (MOFs) to 2D flexible networks via ligand exchange for enhanced CO ₂ /N ₂ and CH ₄ /N ₂ separation. Chemical Communications, 2015, 51, 14716-14719.	4.1	45
100	A novel aided-cation strategy to advance the dehydrogenation of calcium borohydride monoammoniate. Journal of Materials Chemistry, 2012, 22, 5312.	6.7	44
101	Selective electrochemical hydrogenation of furfural to 2-methylfuran over a single atom Cu catalyst under mild pH conditions. Green Chemistry, 2021, 23, 3028-3038.	9.0	43
102	Hydrothermal Synthesis of Metal–Polyphenol Coordination Crystals and Their Derived Metal/Nâ€doped Carbon Composites for Oxygen Electrocatalysis. Angewandte Chemie, 2016, 128, 12658-12662.	2.0	42
103	Phase stability and thermal expansion behavior of Cu6Sn5 intermetallics doped with Zn, Au and In. Intermetallics, 2013, 43, 85-98.	3.9	41
104	Facile Synthesis of Unsolvated Alkali Metal Octahydrotriborate Salts MB ₃ H ₈ (M=K, Rb, and Cs), Mechanisms of Formation, and the Crystal Structure of KB ₃ H ₈ . Angewandte Chemie - International Edition, 2019, 58, 2720-2724.	13.8	39
105	Sustainable S cathodes with synergic electrocatalysis for room-temperature Na–S batteries. Journal of Materials Chemistry A, 2021, 9, 566-574.	10.3	39
106	Novel M (Mg/Ni/Cu)-Al-CO3 layered double hydroxides synthesized by aqueous miscible organic solvent treatment (AMOST) method for CO2 capture. Journal of Hazardous Materials, 2019, 373, 285-293.	12.4	38
107	Manipulating Molecular Structure and Morphology to Invoke Highâ€Performance Sodium Storage of Copper Phosphide. Advanced Energy Materials, 2020, 10, 1903542.	19.5	38
108	The influence of ageing on the stabilisation of interfacial (Cu,Ni)6(Sn,Zn)5 and (Cu,Au,Ni)6Sn5 intermetallics in Pb-free Ball Grid Array (BGA) solder joints. Journal of Alloys and Compounds, 2016, 685, 471-482.	5.5	37

#	Article	IF	CITATIONS
109	Scandium and vanadium borohydride ammoniates: Enhanced dehydrogenation behavior upon coordinative expansion and establishment of Hδ+â<ā^îĤ interactions. Acta Materialia, 2013, 61, 3110-3119.	7.9	35
110	Stabilization of NaZn(BH ₄) ₃ via nanoconfinement in SBA-15 towards enhanced hydrogen release. Journal of Materials Chemistry A, 2013, 1, 250-257.	10.3	34
111	Synthesis, structure and dehydrogenation of zirconium borohydride octaammoniate. Chemical Communications, 2015, 51, 2794-2797.	4.1	34
112	Characterisation of lithium-ion battery anodes fabricated via in-situ Cu6Sn5 growth on a copper current collector. Journal of Power Sources, 2019, 415, 50-61.	7.8	34
113	Synthesis, structures and hydrogen storage properties of two new H-enriched compounds: Mg(BH4)2(NH3BH3)2 and Mg(BH4)2·(NH3)2(NH3BH3). Dalton Transactions, 2013, 42, 14365.	3.3	33
114	Temperature controlled invertible selectivity for adsorption of N2 and CH4 by molecular trapdoor chabazites. Chemical Communications, 2014, 50, 4544.	4.1	33
115	Controlled-Size Hollow Magnesium Sulfide Nanocrystals Anchored on Graphene for Advanced Lithium Storage. ACS Nano, 2018, 12, 12741-12750.	14.6	33
116	Electrochemical Hydrogenation of Furfural in Aqueous Acetic Acid Media with Enhanced 2â€Methylfuran Selectivity Using CuPd Bimetallic Catalysts. Angewandte Chemie - International Edition, 2022, 61, .	13.8	33
117	Epitaxial growth of an atom-thin layer on a LiNi0.5Mn1.5O4 cathode for stable Li-ion battery cycling. Nature Communications, 2022, 13, 1565.	12.8	32
118	Li ⁺ /ZSM-25 Zeolite as a CO ₂ Capture Adsorbent with High Selectivity and Improved Adsorption Kinetics, Showing CO ₂ -Induced Framework Expansion. Journal of Physical Chemistry C, 2018, 122, 18933-18941.	3.1	31
119	Experimental study and thermodynamic evaluation of Mg–La–Zn system. Journal of Alloys and Compounds, 2020, 814, 152297.	5.5	31
120	Three-Dimensional Electronic Network Assisted by TiN Conductive Pillars and Chemical Adsorption to Boost the Electrochemical Performance of Red Phosphorus. ACS Nano, 2020, 14, 4609-4617.	14.6	31
121	Adsorption and visible-light photocatalytic degradation of organic pollutants by functionalized biochar: Role of iodine doping and reactive species. Environmental Research, 2021, 197, 111026.	7.5	31
122	Atomically dispersed S-Fe-N4 for fast kinetics sodium-sulfur batteries via a dual function mechanism. Cell Reports Physical Science, 2021, 2, 100531.	5.6	31
123	Nanoconfinement significantly improves the thermodynamics and kinetics of co-infiltrated 2LiBH4–LiAlH4 composites: Stable reversibility of hydrogen absorption/resorption. Acta Materialia, 2013, 61, 6882-6893.	7.9	30
124	Surface Stabilization of O3-type Layered Oxide Cathode to Protect the Anode of Sodium Ion Batteries for Superior Lifespan. IScience, 2019, 19, 244-254.	4.1	29
125	Properties of CuGa2 Formed Between Liquid Ga and Cu Substrates at Room Temperature. Journal of Electronic Materials, 2020, 49, 128-139.	2.2	29
126	A P3-Type K _{1/2} Mn _{5/6} Mg _{1/12} Ni _{1/12} O ₂ Cathode Material for Potassium-Ion Batteries with High Structural Reversibility Secured by the Mg–Ni Pinning Effect. ACS Applied Materials & Interfaces, 2021, 13, 28369-28377.	8.0	29

#	Article	IF	CITATIONS
127	Metal cation-promoted hydrogen generation in activated aluminium borohydride ammoniates. Acta Materialia, 2013, 61, 4787-4796.	7.9	28
128	Precipitation mechanism of Mg2Ni in Mg-Ni-Y studied by STEM, 3DAP and first-principles calculations. Journal of Alloys and Compounds, 2018, 750, 117-123.	5.5	28
129	A GBH/LiBH4 coordination system with favorable dehydrogenation. Journal of Materials Chemistry, 2011, 21, 7138.	6.7	27
130	A synergistic strategy established by the combination of two H-enriched B–N based hydrides towards superior dehydrogenation. Journal of Materials Chemistry A, 2013, 1, 10155.	10.3	26
131	Phase equilibria of Ce–Mg–Ni ternary system at 673ÂK and hydrogen storage properties of selected alloy. International Journal of Hydrogen Energy, 2016, 41, 1725-1735.	7.1	26
132	Development and Investigation of a NASICONâ€Type Highâ€Voltage Cathode Material for Highâ€Power Sodiumâ€lon Batteries. Angewandte Chemie, 2020, 132, 2470-2477.	2.0	26
133	Nano-confined multi-synthesis of a Li–Mg–N–H nanocomposite towards low-temperature hydrogen storage with stable reversibility. Journal of Materials Chemistry A, 2015, 3, 12646-12652.	10.3	25
134	Confining Ultrathin 2D Superlattices in Mesoporous Hollow Spheres Renders Ultrafast and High apacity Naâ€lon Storage. Advanced Energy Materials, 2020, 10, 2001033.	19.5	25
135	Research Progress and Future Perspectives on Rechargeable Naâ€O ₂ and Naâ€CO ₂ Batteries. Energy and Environmental Materials, 2021, 4, 158-177.	12.8	25
136	Ni segregation in the interfacial (Cu,Ni)6Sn5 intermetallic layer of Sn-0.7Cu-0.05Ni/Cu ball grid array (BCA) joints. Intermetallics, 2014, 54, 20-27.	3.9	24
137	Hydrazine bisborane as a promising material for chemical hydrogen storage. International Journal of Hydrogen Energy, 2011, 36, 13640-13644.	7.1	23
138	In situ study of skim milk structure changes under high hydrostatic pressure using synchrotron SAXS. Food Hydrocolloids, 2018, 77, 772-776.	10.7	23
139	Exploration of the sodium ion ordered transfer mechanism in a MoSe ₂ @Graphene composite for superior rate and lifespan performance. Journal of Materials Chemistry A, 2019, 7, 13736-13742.	10.3	23
140	Ammonia borane modified zirconium borohydride octaammoniate with enhanced dehydrogenation properties. Journal of Materials Chemistry A, 2015, 3, 5299-5304.	10.3	22
141	Nonstoichiometry in Strontium Uranium Oxide: Understanding the Rhombohedral–Orthorhombic Transition in SrUO ₄ . Inorganic Chemistry, 2016, 55, 9329-9334.	4.0	22
142	Effect of extrusion temperature on microstructure, thermal conductivity and mechanical properties of a Mg-Ce-Zn-Zr alloy. Journal of Alloys and Compounds, 2018, 741, 1222-1228.	5.5	22
143	Effect of Zn, Au, and In on the polymorphic phase transformation in Cu ₆ Sn ₅ intermetallics. Journal of Materials Research, 2012, 27, 2609-2614.	2.6	21
144	A comparative study on conversion of porous and non-porous metal–organic frameworks (MOFs) into carbon-based composites for carbon dioxide capture. Polyhedron, 2016, 120, 30-35.	2.2	21

#	Article	IF	CITATIONS
145	A Hydrostable Cathode Material Based on the Layered P2@P3 Composite that Shows Redox Behavior for Copper in Highâ€Rate and Long ycling Sodiumâ€Ion Batteries. Angewandte Chemie, 2019, 131, 1426-1430). ^{2.0}	21
146	Synthesis of Ni5Ga3 catalyst by Hydrotalcite-like compound (HTlc) precursors for CO2 hydrogenation to methanol. Applied Catalysis B: Environmental, 2020, 275, 119067.	20.2	21
147	Comparative analysis of ex-situ and operando X-ray diffraction experiments for lithium insertion materials. Journal of Power Sources, 2016, 302, 126-134.	7.8	20
148	High-Performance Hydrogen Storage Nanoparticles Inside Hierarchical Porous Carbon Nanofibers with Stable Cycling. ACS Applied Materials & amp; Interfaces, 2017, 9, 15502-15509.	8.0	20
149	A Cation and Anion Dual Doping Strategy for the Elevation of Titanium Redox Potential for Highâ€Power Sodiumâ€ion Batteries. Angewandte Chemie, 2020, 132, 12174-12181.	2.0	20
150	Sodium borohydride hydrazinates: synthesis, crystal structures, and thermal decomposition behavior. Journal of Materials Chemistry A, 2015, 3, 11269-11276.	10.3	19
151	Effective Gas Separation Performance Enhancement Obtained by Constructing Polymorphous Core–Shell Metal–Organic Frameworks. ACS Applied Materials & Interfaces, 2019, 11, 30234-30239.	8.0	19
152	Facile Synthesis of Hierarchical Hollow CoP@C Composites with Superior Performance for Sodium and Potassium Storage. Angewandte Chemie, 2020, 132, 5197-5202.	2.0	19
153	Interfacial Reactions between Ga and Cu-10Ni Substrate at Low Temperature. ACS Applied Materials & Interfaces, 2020, 12, 21045-21056.	8.0	19
154	Tuning NaO2 formation and decomposition routes with nitrogen-doped nanofibers for low overpotential Na-O2 batteries. Nano Energy, 2021, 81, 105529.	16.0	19
155	Nitrogen Rejection from Methane via a "Trapdoor―K-ZSM-25 Zeolite. Journal of the American Chemical Society, 2021, 143, 15195-15204.	13.7	19
156	Two novel derivatives of ammonia borane for hydrogen storage: synthesis, structure, and hydrogen desorption investigation. Journal of Materials Chemistry A, 2013, 1, 12263.	10.3	18
157	Revisiting the Hydrogen Storage Behavior of the Na-O-H System. Materials, 2015, 8, 2191-2203.	2.9	18
158	Ultra-narrow-band blue-emitting K2SrBa(PO4)2:Eu2+ phosphor with superior efficiency and thermal stability. Journal of Alloys and Compounds, 2022, 892, 162066.	5.5	18
159	Effect of trace Na additions on the hydrogen absorption kinetics of Mg ₂ Ni. Journal of Materials Research, 2016, 31, 1316-1327.	2.6	17
160	Silica Supported MgO as An Adsorbent for Precombustion CO ₂ Capture. ACS Applied Nano Materials, 2019, 2, 6565-6574.	5.0	17
161	Nanostructured CoS ₂ -Decorated Hollow Carbon Spheres: A Performance Booster for Li-Ion/Sulfur Batteries. ACS Applied Energy Materials, 2020, 3, 6447-6459.	5.1	17
162	Intermetallic formation mechanisms and properties in room-temperature Ga soldering. Journal of Alloys and Compounds, 2020, 826, 154221.	5.5	17

#	Article	IF	CITATIONS
163	Simultaneous quantitative recognition of all purines including N6-methyladenine via the host-guest interactions on a Mn-MOF. Matter, 2021, 4, 1001-1016.	10.0	17
164	Improved dehydrogenation properties of the combined Mg(BH4)2·6NH3–nNH3BH3 system. International Journal of Hydrogen Energy, 2013, 38, 16199-16207.	7.1	16
165	Copper phosphide as a promising anode material for potassium-ion batteries. Journal of Materials Chemistry A, 2021, 9, 8378-8385.	10.3	16
166	Ammonia borane destabilized by aluminium hydride: A mutual enhancement for hydrogen release. International Journal of Hydrogen Energy, 2015, 40, 1047-1053.	7.1	15
167	Li(NH ₃)B ₃ H ₈ : a new ionic liquid octahydrotriborate. Chemical Communications, 2019, 55, 408-411.	4.1	15
168	Structure tailoring and defect engineering of LED phosphors with enhanced thermal stability and superior quantum efficiency. Chemical Engineering Journal, 2022, 435, 133873.	12.7	15
169	Pressureâ€Induced Intersite BiM (M=Ru,â€Ir) Valence Transitions in Hexagonal Perovskites. Angewandte Chemie - International Edition, 2014, 53, 3414-3417.	13.8	14
170	Controlling Oxygen Defect Formation and Its Effect on Reversible Symmetry Lowering and Disorder-to-Order Phase Transformations in Nonstoichiometric Ternary Uranium Oxides. Inorganic Chemistry, 2019, 58, 6143-6154.	4.0	14
171	Understanding Local Bonding Structures of Ni-Doped Chromium Nitride Coatings through Synchrotron Radiation NEXAFS Spectroscopy. Journal of Physical Chemistry C, 2014, 118, 18573-18579.	3.1	13
172	Metalâ€Borohydrideâ€Modified Zr(BH ₄) ₄ â‹8 NH ₃ : Lowâ€Tempera Dehydrogenation Yielding Highly Pure Hydrogen. Chemistry - A European Journal, 2015, 21, 14931-14936.	ture 3.3	13
173	Pd(0) loaded Zn ₂ (azoBDC) ₂ (dabco) as a heterogeneous catalyst. CrystEngComm, 2017, 19, 4182-4186.	2.6	13
174	2D Titania–Carbon Superlattices Vertically Encapsulated in 3D Hollow Carbon Nanospheres Embedded with 0D TiO 2 Quantum Dots for Exceptional Sodiumâ€ion Storage. Angewandte Chemie, 2019, 131, 14263-14266.	2.0	13
175	Rapid Lithium Insertion and Location of Mobile Lithium in the Defect Perovskite Li _{0.18} Sr _{0.66} Ti _{0.5} Nb _{0.5} O ₃ . ChemPhysChem, 2012, 13, 2293-2296.	2.1	12
176	Synthesis of ammine dual-metal (V, Mg) borohydrides with enhanced dehydrogenation properties. International Journal of Hydrogen Energy, 2013, 38, 5322-5329.	7.1	12
177	Study on Vanadium Substitution to Iron in Li2FeP2O7 as Cathode Material for Lithium-ion Batteries. Electrochimica Acta, 2014, 141, 195-202.	5.2	12
178	In situsynchrotron X-ray diffraction investigation ofÂthe evolution of a PbO2/PbSO4surface layer onÂaÂcopper electrowinning Pb anode in a novel electrochemical flow cell. Journal of Synchrotron Radiation, 2015, 22, 366-375.	2.4	12
179	Kinetics of the β → α Transformation of Tin: Role of α-Tin Nucleation. Crystal Growth and Design, 2015, 15, 5767-5773.	3.0	12
180	Retrogradation of Maize Starch after High Hydrostatic Pressure Gelation: Effect of Amylose Content and Depressurization Rate. PLoS ONE, 2016, 11, e0156061.	2.5	12

#	Article	IF	CITATIONS
181	Understanding Performance Differences from Various Synthesis Methods: A Case Study of Spinel LiCr _{0.2} Ni _{0.4} Mn _{1.4} O ₄ Cathode Material. ACS Applied Materials & Interfaces, 2016, 8, 26051-26057.	8.0	12
182	The effects of Ni on inhibiting the separation of Cu during the lithiation of Cu6Sn5 lithium-ion battery anodes. Journal of Power Sources, 2019, 440, 227085.	7.8	12
183	Thermodynamic assessment of Mgâ^'Niâ^'Y system focusing on long-period stacking ordered phases in the Mg-rich corner. Journal of Magnesium and Alloys, 2022, 10, 3250-3266.	11.9	12
184	Temperature and composition dependent structural investigation of the defect perovskite series Sr1â^'xTi1â^'2xNb2xO3, 0â‰ ¤ â‰ 0 .2. Journal of Solid State Chemistry, 2010, 183, 1998-2003.	2.9	11
185	Influence of Ti and La Additions on the Formation of Intermetallic Compounds in the Al-Zn-Si Bath. Metallurgical and Materials Transactions A: Physical Metallurgy and Materials Science, 2016, 47, 6542-6554.	2.2	11
186	Monovalent Cation–Phenolic Crystals with pHâ€Driven Reversible Crystal Transformation. Chemistry - A European Journal, 2019, 25, 12281-12287.	3.3	11
187	Phosphorusâ€Modulationâ€Triggered Surface Disorder in Titanium Dioxide Nanocrystals Enables Exceptional Sodiumâ€6torage Performance. Angewandte Chemie, 2019, 131, 4062-4066.	2.0	11
188	Electrocatalytic-driven compensation for sodium ion pouch cell with high energy density and long lifespan. Energy Storage Materials, 2021, 39, 54-59.	18.0	11
189	Effect of trace Na additions on the hydriding kinetics of hypo-eutectic Mg–Ni alloys. International Journal of Hydrogen Energy, 2017, 42, 6851-6861.	7.1	10
190	Effects of Ni and Cu Antisite Substitution on the Phase Stability of CuGa2 from Liquid Ga/Cu–Ni Interfacial Reaction. ACS Applied Materials & Interfaces, 2019, 11, 32523-32532.	8.0	10
191	Hydrangea-Shaped 3D Hierarchical Porous Magnesium Hydride–Carbon Framework with High Rate Performance for Lithium Storage. ACS Applied Materials & Interfaces, 2019, 11, 28987-28995.	8.0	10
192	Conjugated crosslinks boost the conductivity and stability of a single crystalline metal–organic framework. Chemical Communications, 2021, 57, 187-190.	4.1	10
193	The effect of Na addition on the first hydrogen absorption kinetics of cast hypoeutectic Mg–La alloys. International Journal of Hydrogen Energy, 2021, 46, 27096-27106.	7.1	10
194	Na-modified cast hypo-eutectic Mg–Mg2Si alloys for solid-state hydrogen storage. Journal of Power Sources, 2022, 538, 231538.	7.8	10
195	The crystal structure, microhardness and thermal stability of the Ti26Al55Zn19 alloy. Intermetallics, 2012, 26, 136-141.	3.9	9
196	Valence changes of manganese and structural phase transitions in Sr1â^'xPrxMnO3 (0.1â‰ ¤ â‰ 0 .6). Journal of Solid State Chemistry, 2013, 201, 115-127.	2.9	9
197	Aluminum Borohydride Complex with Ethylenediamine: Crystal Structure and Dehydrogenation Mechanism Studies. Journal of Physical Chemistry C, 2016, 120, 10192-10198.	3.1	9
198	Rapid fabrication of tin-copper anodes for lithium-ion battery applications. Journal of Alloys and Compounds, 2021, 867, 159031.	5.5	9

#	Article	IF	CITATIONS
199	Electrochemical Hydrogenation of Furfural in Aqueous Acetic Acid Media with Enhanced 2â€Methylfuran Selectivity Using CuPd Bimetallic Catalysts. Angewandte Chemie, 2022, 134, .	2.0	9
200	New High-Pressure Polymorph of the Nonlinear Optical Crystal BaTeMo ₂ O ₉ . Crystal Growth and Design, 2015, 15, 3110-3113.	3.0	8
201	X-ray diffraction investigation of amorphous calcium phosphate and hydroxyapatite under ultra-high hydrostatic pressure. International Journal of Minerals, Metallurgy and Materials, 2015, 22, 1225-1231.	4.9	8
202	Novel structurally-stable Na-rich Na ₄ V ₂ O ₇ cathode material with high reversible capacity by utilization of anion redox activity. Chemical Communications, 2020, 56, 8245-8248.	4.1	8
203	The decomposition of α-LiN ₂ H ₃ BH ₃ : an unexpected hydrogen release from a homopolar proton–proton pathway. Journal of Materials Chemistry A, 2014, 2, 15627.	10.3	7
204	Tailoring phase transition temperatures in perovskites via A-site vacancy generation. Dalton Transactions, 2017, 46, 7253-7260.	3.3	7
205	A new indium selenide phase: controllable synthesis, phase transformation and photoluminescence properties. Journal of Materials Chemistry C, 2019, 7, 13573-13584.	5.5	7
206	Boosting capacity and operating voltage of LiVO3 as cathode for lithium-ion batteries by activating oxygen reaction in the lattice. Journal of Power Sources, 2022, 517, 230728.	7.8	7
207	Hydrogen sorption behaviour of Mg-5wt.%La alloys after the initial hydrogen absorption process. International Journal of Hydrogen Energy, 2022, 47, 16132-16143.	7.1	7
208	Synthesis and advanced dehydrogenation properties of niobium-based ammine borohydride. International Journal of Hydrogen Energy, 2013, 38, 9236-9242.	7.1	6
209	Exchange Method Using Acid‧olvent Synergy for Metal–Organic Framework Synthesis (EASYâ€MOFs) Based on a Typical Pillar‣ayered Parent Structure. European Journal of Inorganic Chemistry, 2016, 2016, 1466-1469.	2.0	6
210	Inhibitory effect of Ti and La on Fe dissolution in Al–Zn–Si bath by in-situ SXRD, SXRF, TEM and DFT calculation. Materials Characterization, 2018, 145, 135-141.	4.4	6
211	Interfacial reactions between Ga and Cu-xNi (x=0, 2, 6, 10, 14) substrates and the strength of Cu-xNi/Ga/Cu-xNi joints. Intermetallics, 2021, 133, 107168.	3.9	6
212	Electrical Regulation of CO ₂ Adsorption in the Metal–Organic Framework MIL-53. ACS Applied Materials & Interfaces, 2022, 14, 13904-13913.	8.0	6
213	Synchrotron X-ray Powder Diffraction for Fast, In-Situ Insights. Synchrotron Radiation News, 2014, 27, 18-20.	0.8	5
214	Dehydrogenation properties of chromium-based ammine borohydrides: CrCl3•nNH3/3LiBH4 (nÂ=Â3, 4 and) Tj E	TQ <u>q</u> 0 0 0	rg&T /Overlo

215	Electrochemically enhanced Cu6Sn5 anodes with tailored crystal orientation and ordered atomic arrangements for lithium-ion battery applications. Acta Materialia, 2020, 201, 341-349.	7.9	5
216	In-situ SAXS investigation of high-pressure triglyceride polymorphism in milk cream and anhydrous milk fat. LWT - Food Science and Technology, 2021, 135, 110174.	5.2	5

#	Article	IF	CITATIONS
217	First Observation of Low-Temperature Magnetic Transition in CuAgSe. Journal of Physical Chemistry C, 2018, 122, 19139-19145.	3.1	4
218	Graphene confined intermetallic magnesium silicide nanocrystals with highly exposed (2 2 0) facets for anisotropic lithium storage. Chemical Engineering Journal, 2021, 419, 129660.	12.7	4
219	Coupling of Jahn–Teller and tilting distortions in high temperature structural phase transition of the Ca0.2Sr0.6Nd0.2Mn1â^'xCrxO3; 0Ââ‰ÂxÂâ‰Â0.2 perovskites. Solid State Sciences, 2012, 14, 506-514.	3.2	3
220	A synchrotron X-ray powder diffraction and step potential electrochemical spectroscopy study on the change in manganese dioxide capacitive behaviour during cycling. Electrochimica Acta, 2018, 260, 630-639.	5.2	3
221	Theoretical Study of Moisture-Pretreated Lithium as Potential Material for Natural Gas Upgrading. Industrial & Engineering Chemistry Research, 2018, , .	3.7	3
222	A Flow-Through Reaction Cell for Studying Minerals Leaching by In-Situ Synchrotron Powder X-ray Diffraction. Minerals (Basel, Switzerland), 2020, 10, 990.	2.0	3
223	Synthesis, structure and dielectric properties of the Sr ₃ Ti _{1â^'x} Zr _x Nb ₄ O ₁₅ , (0 ≤i>x ≤), series of tungsten bronze type compounds. CrystEngComm, 2020, 22, 4994-5001.	2.6	3
224	Crystal structure of propionitrile (CH ₃ CH ₂ CN) determined using synchrotron powder X-ray diffraction. Journal of Synchrotron Radiation, 2020, 27, 212-216.	2.4	3
225	The Effects of Trace Sb and Zn Additions on Cu6Sn5 Lithium-Ion Battery Anodes. Journal of Nanoscience and Nanotechnology, 2020, 20, 5182-5191.	0.9	3
226	Controlled Hydrolysis of TiO ₂ from HCl Digestion Liquors of Ilmenite. Industrial & Engineering Chemistry Research, 2022, 61, 6333-6342.	3.7	3
227	Combination of two H-enriched B–N based hydrides towards improved dehydrogenation properties. International Journal of Hydrogen Energy, 2014, 39, 11668-11674.	7.1	2
228	Effect of impurity N2 concentration on the hydriding kinetics of Na-doped Mg–Ni alloys. International Journal of Hydrogen Energy, 2017, 42, 366-375.	7.1	2
229	Transitionâ€Metalâ€Containing Porphyrin Metal–Organic Frameworks as Ï€â€Backbonding Adsorbents for NO 2 Removal. Angewandte Chemie, 2020, 132, 19848-19851.	2.0	2
230	Compressibility of Al64Pd30.4Fe5.6. Zeitschrift Fur Kristallographie - Crystalline Materials, 2009, 224, 119-122.	0.8	2
231	Investigation on the Solidification and Phase Transformation in Pb-Free Solders Using In Situ Synchrotron Radiography and Diffraction: A Review. Acta Metallurgica Sinica (English Letters), 2022, 35, 49-66.	2.9	2
232	The role of π-bonding on the high temperature structure of the double perovskites Ba ₂ CaUO ₆ and BaSrCaUO ₆ . Dalton Transactions, 2015, 44, 16036-16044.	3.3	1
233	Squeezing electrons out of 6s2 lone-pairs in perovskite-type oxides. Chemical Communications, 2019, 55, 3887-3890.	4.1	1
234	lon-transport phenomena and anomalous transformations in strontium uranium oxides. Acta Crystallographica Section A: Foundations and Advances, 2017, 73, C1428-C1428.	0.1	0

#	Article	IF	CITATIONS
235	Facility upgrades at the Australian Synchrotron: extending the powder diffraction capabilities. Acta Crystallographica Section A: Foundations and Advances, 2019, 75, e729-e729.	0.1	0